ACS APPLIED MATERIALS & INTERFACES

Research Article

www.acsami.org

Facile Synthesis of Spike-Piece-Structured $Ni(OH)_2$ Interlayer Nanoplates on Nickel Foam as Advanced Pseudocapacitive Materials for Energy Storage

Li Chen Wu, Yue Jiao Chen, Ming Lei Mao, Qiu Hong Li,* and Ming Zhang*

College of Materials Science and Engineering, Key Laboratory for Micro−Nano Optoelectronic Devices of Ministry of Education, and State Key Laboratory for Chemo/Biosensing and Chemometrics, Hunan University, Changsha 410082, People's Republic of China

ABSTRACT: The spike-piece-structured $Ni(OH)_2$ multilayer nanoplate arrays on nickel foams are directly synthesized by a facile hydrothermal method at 160 °C for 4 h. A possible mechanism for the growth of those nanostructures is proposed based on the experimental results. It is discovered that the surface of nickel foams could affect the orientation of the $Ni(OH)_2$ nanoplates. This unique multilayer nanoplate array structure significantly enhances the electroactive surface areas of $Ni(OH)_2$, leading to shorter ion-diffusion paths, and displays a capacity of 2.83 F/cm^2 at a current density of 6 mA/cm^2 in 0−0.48 V versus the saturated calomel electrode. It also exhibits a good cycling performance, with 51.5% of its initial capacity after about 3000 cycles at a large current density of 24 mA/cm^2. The present results may provide a new strategy for the synthesis and application of nickel-foam-based composites for energy storage.

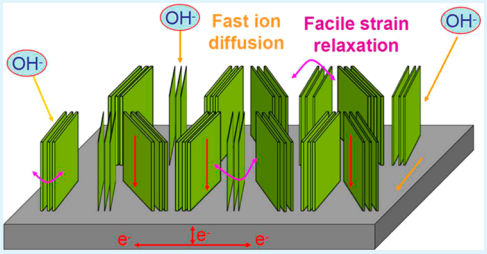

KEYWORDS: *nickel hydroxides, nickel foams, hydrothermal synthesis, supercapacitors*

1. INTRODUCTION

Supercapacitors as high-performance devices for energy storage have attracted great interest because of their high power density, long cycle life, and low maintenance cost.[1−4] The mechanisms of supercapacitors include two types: ion adsorption (electrochemical double-layer capacitors, EDLCs) and fast surface redox reactions (pseudocapacitors).[5−7] Limited by the specific surface area of the electrode materials, EDLCs cannot meet the ever-growing demand for peak power density in electric vehicles. Thus, great attention in supercapacitors has been paid to pseudocapacitors because their specific capacity is substantially larger than that of EDLCs.[8,9] Traditionally, the most notable pseudocapacitive material is RuO_2.[10,11] However, the very high cost and rareness of the Ru element greatly hinder its application at large scale. Nowadays, lots of alternative materials have been studied as pseudocapacitor electrodes, such as transition-metal oxides, metal hydroxides, and polymeric materials.[12−14] Among them, $Ni(OH)_2$ is a particularly promising material because of its well-defined electrochemical redox activity, high capacitance, and low cost.[15−19]

In recent years, a large number of studies have been launched on $Ni(OH)_2$ nanomaterials because of their high surface-to-volume ratio and convenient transport channels for electrolyte ions.[20−22] To achieve the high power density and energy density of $Ni(OH)_2$-based supercapacitors, a compromise between the volume density of $Ni(OH)_2$ (to achieve a high specific volume capacitance) and their specific surface area as well as porosity (to ensure high capacitance and easy access to the electrolyte) should be reached to realize the fast storage of energy in a relatively small volume. According to this strategy, much attention has been devoted to preparing $Ni(OH)_2$/nickel foam (NF) composites.[8,23,24] For example, $Ni(OH)_2$ with porous and 3D nanostructure was electrodeposited on NFs to synthesize the composites.[23] In another study, a hydrothermal route was employed to deposit ultrathin primary nanowalls of $Ni(OH)_2$ on NFs, and the composites showed a capacitance higher than the theoretical value.[8] Chemical bath deposition also could be used to prepare the $Ni(OH)_2$/NF composites.[24] Various kinds of $Ni(OH)_2$ nanostructures, including hollow spheres, nanofibers, nanotubes, nanoflakes, and nanosheets, have been achieved.[12,25−29] In spite of this, few researchers have investigated the relationship between the NFs and $Ni(OH)_2$ and the effects of the area density of $Ni(OH)_2$ in the $Ni(OH)_2$/NFs on their performances.

In this paper, multilayer $Ni(OH)_2$ nanoplate arrays on NFs with some interspace among them were prepared by a facile hydrothermal route. The effects of the surface of NFs on the morphology of $Ni(OH)_2$ nanoplate arrays were investigated in detail. A possible mechanism for the synthesis of $Ni(OH)_2$ nanoplate arrays was proposed based on the time-dependent experiments. This unique and novel nanoarchitecture displays a capacitance of 2.83 F/cm^2 at a current density of 6 mA/cm^2. Also, it remained about 51.5% of its initial capacity after 3000 cycles at a large current density of 24 mA/cm^2. Compared with the arrays composed of single layer $Ni(OH)_2$, the multilayer nanoplate arrays in this study significantly enhanced the electroactive surface areas, leading to effective interfacial/chemical distributions at nanoscale and fast ion and electron

Received: January 21, 2014
Accepted: March 5, 2014
Published: March 5, 2014

transfer. The electrolyte could easily contact with the $Ni(OH)_2$ surface throughout the NF network and then access the inner region of $Ni(OH)_2$ nanoplates. Furthermore, the interspaces between the nanoplate arrays contributed to facile strain relaxation, alleviating the structure or phase damage caused by redox reaction during the charge/discharge cycles. All of these characteristics reveal that these multilayer-structured $Ni(OH)_2$ arrays are promising candidates for electrochemical energy storage.

2. EXPERIMENTAL SECTION

Preparation of $Ni(OH)_2$ Arrays. The $Ni(OH)_2$ nanoplate arrays were prepared by a hydrothermal synthesis technique. All of the chemicals were of analytical grade and were used without further purification. In a typical procedure, 1 mmol of $Ni(NO_3)_2{\cdot}6H_2O$ (0.291 g), 4 mmol of carbamide (0.240 g), and 2 mmol of NH_4F (0.074 g) were dissolved in 40 mL of deionized water and stirred in a magnetic stirring apparatus to form a clear solution. All of the NFs in this study were cut from a large piece of NF with a thickness of 1 mm. Pieces of NF with the size of 2 × 2 cm^2 were carefully cleaned using a 2 M HCl solution in an ultrasonic bath for 30 min in order to remove the surface oxide layer,[8] and then they were cleaned in deionized water, absolute ethanol, and acetone for 15 min in sequence by ultrasonication. Drying and weighing of the NFs were performed after all of these cleaning processes were completed. The mixed solution and the clean NFs were transferred to four sealed 50 mL Teflon-lined stainless steel autoclaves and maintained at 160 °C for 4 h. Then they were cooled to room temperature by cooling water. $Ni(OH)_2$ on the NFs was swilled for 10 min by both distilled water and ethanol assisted by ultrasonication, dried at 60 °C, and then weighed again. For exploration of the effects of the surface of NFs on the product morphology, several NF pieces were also cleaned using 0, 0.2, and 0.8 M HCl with the help of an ultrasonic bath for 30 min and then reacted at 160 °C for 0.5 h with the mixed solution. To investigate the growth process, products were also collected at reaction times of 0.5, 1, and 6 h, respectively, and other conditions were the same as those of the product at 4 h.

Characterization of $Ni(OH)_2$ Arrays. Powder X-ray diffraction (XRD) patterns were recorded on an X-ray diffractometer [Siemens D-5000 diffractometer with Cu Kα irradiation (λ = 1.5406 Å)]. The morphology of the samples was investigated by scanning electron microscopy (SEM; Hitachi S4800) and high-resolution transmission electron microscopy (TEM; JEOL 2010 system operated) at 200 kV.

Electrochemical Measurements of $Ni(OH)_2$ Arrays. The electrochemical measurements were carried out at 298 K in a three-electrode system connected to an electrochemical workstation. $Ni(OH)_2$ on the NFs (1 × 1 cm^2) was used as a working electrode. A platinum foil and a saturated calomel electrode were used as the counter and reference electrodes, respectively. Also, the fresh 2 M KOH aqueous solution was used as the electrolyte. Cyclic voltammetry (CV) measurements were performed on a CHI660d electrochemical workstation (Chenhua, Shanghai).

The specific capacitance (C), energy density (E), and power density (P) were calculated according to the equations

$$C = I\Delta t/s\Delta V \quad (1)$$

$$E = C\Delta V^2/2 \quad (2)$$

$$P = E/\Delta t \quad (3)$$

where I (A) represents the discharge current and s (cm^2), ΔV (V), and Δt (s) designate the surface area of active materials, potential drop during discharge, and total discharge time, respectively.

3. RESULTS AND DISCUSSION

The phase identification and morphology of the synthesized samples were examined by SEM and XRD. The SEM images of the $Ni(OH)_2$ arrays at 4 h at different magnifications are shown in Figure 1. Figure 1a reveals that each plate is composed of a stack of thinner slices with small gaps between them. Figure 1b

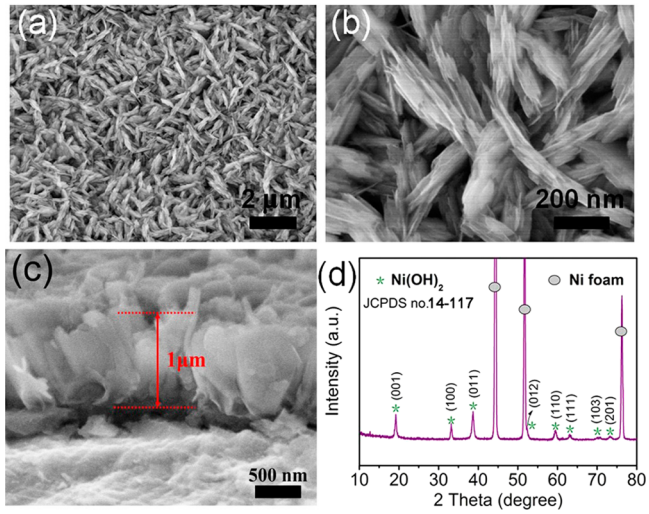

Figure 1. (a) Low-magnification and (b) high-magnification SEM images of $Ni(OH)_2$ nanoplate arrays grown in 4 h. (c) Cross-sectional view of the $Ni(OH)_2$ arrays (4 h). (d) XRD patterns of the $Ni(OH)_2$ nanoplate arrays (4 h) before cycling testing.

shows that the $Ni(OH)_2$ sample is a spike-piece-structured nanoplate with a width of 70−100 nm. It seems that the nanoplates were assembled from very thin nanoplates. Figure 1c is the cross-sectional view of the $Ni(OH)_2$ arrays, in which the thickness of the sample is estimated to be 1 μm. The dense $Ni(OH)_2$ nanoplates on NFs after ultrasonic treatment show that they are firmly fixed on the NFs. As shown in Figure 1d, the XRD pattern can be indexed to $Ni(OH)_2$ (JCPDS no. 14-117), and the peaks marked as "○" come from the NF substrate. The relatively high peaks of $Ni(OH)_2$ are intense, indicating that the samples are of high crystallinity, which is consistent with the TEM results below.[2,30]

After the green films were scraped from the NFs and dispersed in ethanol under ultrasound, the $Ni(OH)_2$ nanoplates (4 h) were examined by TEM, as shown in Figure 2. The high-magnification TEM images show that the nanoplates exhibit

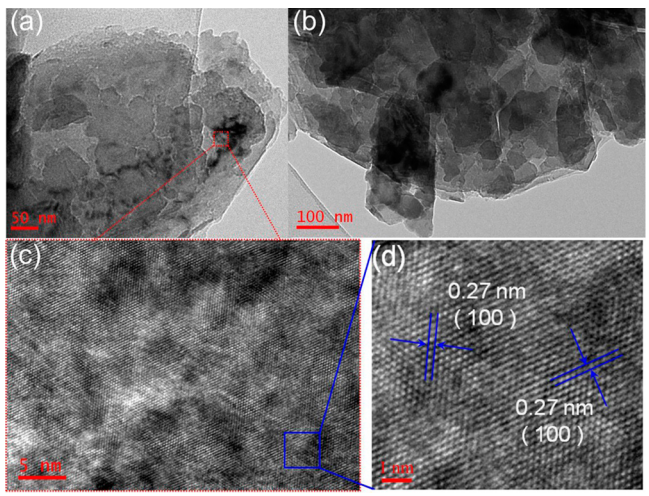

Figure 2. (a and b) Low-magnification and (c and d) high-magnification TEM images of $Ni(OH)_2$ nanoplate arrays (4 h).

dx.doi.org/10.1021/am500449b | ACS Appl. Mater. Interfaces 2014, 6, 5168−5174

irregular shapes (Figure 2a,b) and distribute nonuniformly. The obvious and regular dots in Figure 2c indicate that $Ni(OH)_2$ nanoplates are well-crystallized. The distance between the lattice fringes is approximately 0.27 nm (Figure 2d), corresponding to the (100) plane of $Ni(OH)_2$ and matching well with the XRD results.

SEM images of products grown on NFs treated by different concentrations of HCl are presented in Figure 3. Parts a–d of Figure 3 correspond to the conditions of 0, 0.2, 0.8, and 2 M HCl, respectively. No obvious platelike $Ni(OH)_2$ was generated on the NFs without the HCl treatment in Figure 3a. When the concentration of HCl was increased to 0.2 M, a platelike structure absolutely formed and parts of the plates were parallel to each other (Figure 3b). With the concentration of HCl was adjusted to 0.8 M, the parallel plates decreased and began to mutually cross (Figure 3c). As the concentration of HCl was further increased to 2 M, the plates became fully interlaced with each other (Figure 3d). Thereby, the product morphology can be effected by the surface of the NFs corroded by different concentrations of HCl, which may produce lots of active sites for growing $Ni(OH)_2$ nanoplates. The above phenomenon may be explained as follows. There were some impurities on the NFs. The $Ni(OH)_2$ nanoplates would not be fixed on the NFs if the impurities on the surface were not cleared up. After the impurities were removed by a HCl solution (0.2–0.8 M), the $Ni(OH)_2$ nanoplates could be deposited on NiO on the surface of the NFs. Because the *d* value (0.241 nm) of the (111) plane of NiO (JCPDS no. 47-1049) is very close to that (0.233 nm) of the (101) plane of $Ni(OH)_2$ (JCPDS no. 14-117), NiO on the surface of the NFs may affect the morphology of the $Ni(OH)_2$ nanoplates. When NiO was completely removed by a HCl solution (2 M), the $Ni(OH)_2$ nanoplates were directly fixed onto the Ni. Because none of the main *d* value of Ni (JCPDS no. 4-850) is close to those of $Ni(OH)_2$ (JCPDS no. 14-117), the growth of $Ni(OH)_2$ nanoplates on NFs could not be affected by the Ni. So, the $Ni(OH)_2$ nanoplates on NFs were irregular. Besides, electron transfer between the $Ni(OH)_2$ nanoplates and NFs would become more favorable without transportation of NiO.

To explain the forming process of spike-piece-structured $Ni(OH)_2$ interlayer nanoplate arrays on NFs, the time-dependent reaction was terminated at 0.5, 1, 4, and 6 h. The mass loading of $Ni(OH)_2$ was 1, 1.4, 2, and 2.2 mg on the NFs (1×1 cm^2) grown in 0.5, 1, 4, and 6 h, respectively. SEM images of the samples are shown in Figure 4a–d, and the corresponding schematic illustration for the $Ni(OH)_2$ array growing process on the NFs is also displayed in Figure 4e–h, which is speculated to follow an anisotropic growth self-assembly mechanism. After treatment by a hydrothermal route for 0.5 h, the very thin plates were deposited on the NFs. When the reaction reached 1 h, the interlaced $Ni(OH)_2$ became thicker and larger. When the reaction time was increased to 4 h, those single plates spontaneously evolved into spike-piece $Ni(OH)_2$ architecture. After reaction for 6 h, the spike-piece $Ni(OH)_2$ nanoplates moved closer to each other with decreasing interspace, accompanied by spare slices between spike-piece plates. On the basis of the experimental results, a possible morphological evolution mechanism of the $Ni(OH)_2$ nanoplate arrays was proposed. It can be explained that the surface energy of an individual nanoplate is extraordinarily high. In order to minimize the overall surface energy, the single plate tends to self-assemble spontaneously to form spike-piece-structured $Ni(OH)_2$ interlayer nanoplate arrays on the NFs as the reaction continues further.[28]

The electrochemical properties of the $Ni(OH)_2$ nanoplate arrays (obtained at 4 h) were characterized by CV. The CV curves recorded at different scan rates in a 2 M KOH aqueous solution are shown in Figure 5a. A pair of strong redox peaks can be found in each CV curve, indicating that the capacitance

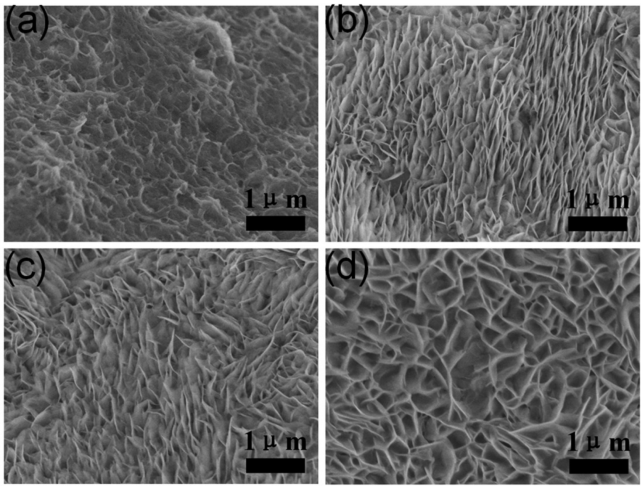

Figure 3. $Ni(OH)_2$ nanoplate arrays (0.5 h) made on various NFs cleaned by different concentrations of a HCl solution: (a) 0 M; (b) 0.2 M; (c) 0.8 M; (d) 2 M.

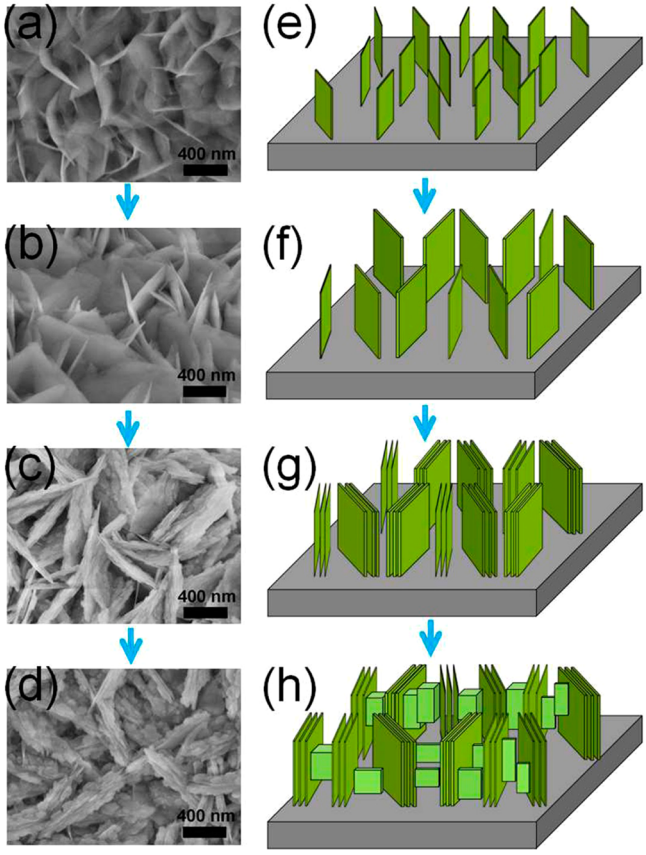

Figure 4. Schematic illustration and corresponding SEM images for the $Ni(OH)_2$ nanoplate arrays growing on the NFs: (a and e) 0.5 h; (b and f) 1 h; (c and g) 4 h; (d and h) 6 h.

dx.doi.org/10.1021/am500449b | ACS Appl. Mater. Interfaces 2014, 6, 5168–5174

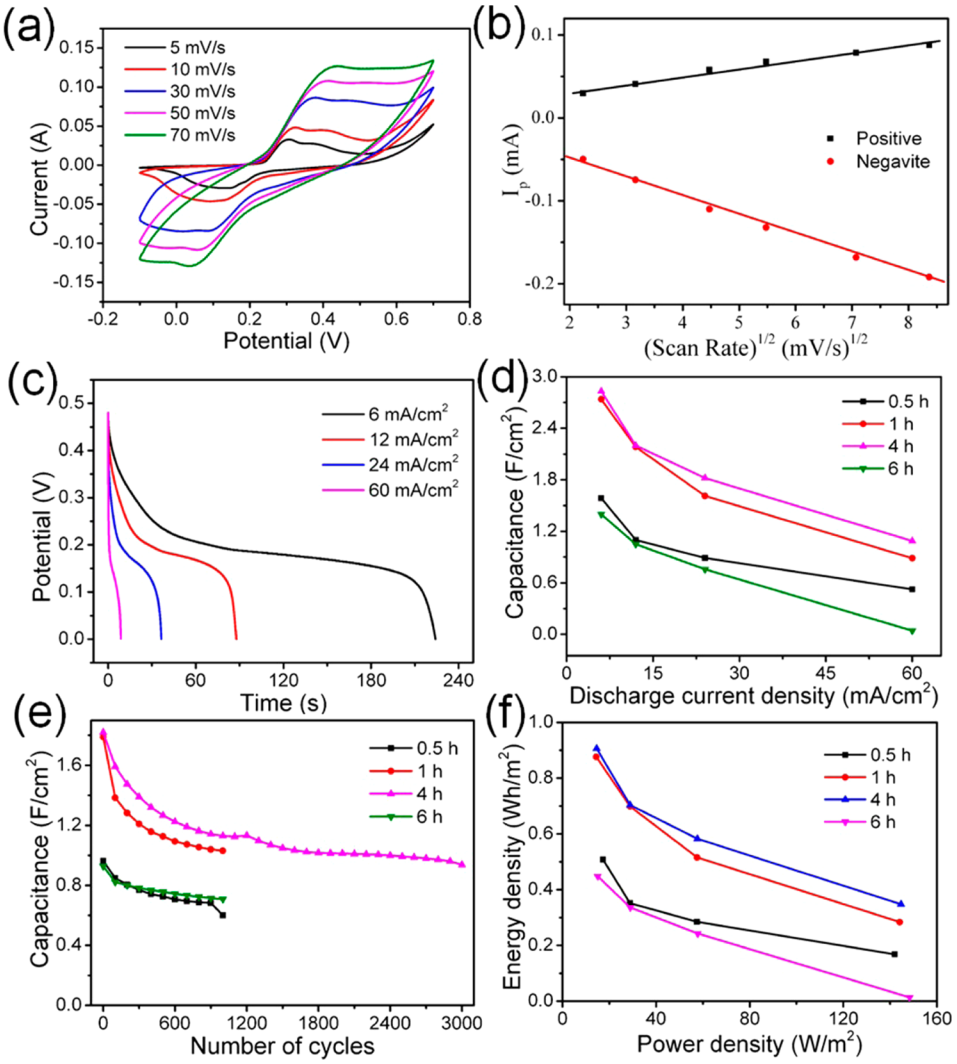

Figure 5. Electrochemical characterizations of the $Ni(OH)_2$ nanoplate arrays. (a) CV curves at different scan rates for the $Ni(OH)_2$ nanoplate arrays (4 h). (b) Relationship between the peak currents and the square root of the corresponding scan rates in CV curves (part a). (c) Discharge curves at various current densities for the $Ni(OH)_2$ nanoplate arrays (4 h). (d) Specific capacitance versus discharge current densities for $Ni(OH)_2$ nanoplate arrays obtained at different reaction times. (e) Cyclic performance of $Ni(OH)_2$ nanoplate arrays obtained at different reaction times at 24 mA/cm^2. (f) Ragone plot of the energy density and power density at various charge/discharge rates.

characteristic is mainly governed by Faradaic redox reactions, which is obviously distinct from that of EDLCs whose CV curve usually exhibits an ideal rectangular shape.[24,25] The anodic oxidation peak is attributed to the conversion of nickel hydroxide to nickel oxyhydroxide, while the reduction peak is associated with its reverse process. The electrochemical reaction can be expressed as follows:[31]

$$Ni(OH)_2 + OH^- \rightleftharpoons NiOOH + H_2O + e^- \quad (4)$$

The area included in the CV curve can be used to estimate the capacitance of the system.[27,32] The current increases with the scan rate, while the specific capacitance decreases gradually with an increase in the scan rate, which can be ascribed to the diffusion effect. At high scan rates, diffusion and migration of the electrolyte ions within the electrode are limited, resulting in low electrochemical utilization of the $Ni(OH)_2$ material. With increasing scan rates, the potential of the oxidation peak shifts in the positive direction and that of the reduction peak shifts in the negative direction, which is mainly associated with the internal resistance of the electrode.[33] A linear relationship between the current of the redox peaks in the CV curves at different scan rates and the square root of the corresponding scan rate is shown in Figure 5b, indicating that the redox reaction is a diffusion-controlled process.[4] Therefore, the irregular $Ni(OH)_2$ nanoplate arrays are a benefit for the diffusion of ions, maybe resulting in their improved electrochemical properties.

The discharge curves of the $Ni(OH)_2$ electrode (grown for 4 h) at different current densities are shown in Figure 5c. Unlike the linear characteristic of EDLCs, the discharge curves of the $Ni(OH)_2$ electrode exhibit typical pseudocapacitive behavior, which agrees well with its CV result.[32] As the discharge current density increases, the specific capacitance decreases to a large degree. This phenomenon is probably related to the diffusion process of OH^- ions during the charge–discharge cyclic process of the electrode. The limited OH^- ions cannot meet well with the need of higher current densities, in which more OH^- ions are required to intercalate swiftly at the electrode–electrolyte interface.[34,35]

dx.doi.org/10.1021/am500449b | ACS Appl. Mater. Interfaces 2014, 6, 5168–5174

Figure 5d displays the specific capacitance of the $Ni(OH)_2$ nanoplate arrays generated at various times at different current densities. The specific capacitance of $Ni(OH)_2$ formed in 4 h is obviously higher than those of $Ni(OH)_2$ obtained at other times. It displays a maximum capacitance of 2.83 F/cm^2 at a current density of 6 mA/cm^2. Although the specific capacitance decreased with an increase in the discharge current density, the specific capacitance still remains 1.82 F/cm^2 at 24 mA/cm^2, 64.3% of the maximum capacitance. The unique spike-piece $Ni(OH)_2$ structure (formed in 4 h), which is composed of a stack of highly closed nanoflakes, endows the sample with large specific surface area, resulting in a high specific capacitance. The $Ni(OH)_2$ nanoplates grown in 0.5 and 1 h are loose and almost single. So, the specific capacitance of the $Ni(OH)_2$ nanoplates increases along with the reaction time and mass loading of $Ni(OH)_2$. When the reaction time was extended to 6 h, the $Ni(OH)_2$ nanoplates stacked together and the interspace among the nanoplates were filled with $Ni(OH)_2$ particles (Figure 4d), leading to an increase in the diffusion distance and a decrease in the diffusion rates of ions. Therefore, the specific capacitance of the $Ni(OH)_2$ nanoplates obtained at 6 h is much lower than that of the samples obtained at 1 h, especially at a large current density (Figure 5d).

The cycle characteristics of $Ni(OH)_2$ were also examined, and the results are shown in Figure 5e. The specific capacitance of $Ni(OH)_2$ formed in 4 h remains only 62.1% (1.1 F/cm^2) of its initial capacity after 1000 cycles at 24 mA/cm^2. Obviously, this value is always higher than that of other times during the 1000 cycles. After 3000 cycles, the $Ni(OH)_2$ sample (4 h) remains 51.5% (about 0.95 F/cm^2) of the initial capacitance, showing an improved specific capacitance and a superior cyclic stability. Those areal capacitances are higher than those of previous results about $Ni(OH)_2$ on NFs, as shown in Table 1.

Table 1. Electrochemical Properties of $Ni(OH)_2$ and Some Other Materials on Various Substrates

material	substrate	capacitance (F/cm^2)	ref
$Ni(OH)_2$	NFs	0.7	32
$Ni(OH)_2$	NFs	0.7	38
$Ni(OH)_2$	graphene	0.9	36
$Ni(OH)_2$	graphene	0.003	10
$Ni(OH)_2/NiCo_2O_4$	CFP[a]	5.2	7
$Ni(OH)_2/Co_3O_4$	CFP	3.3	7
NiO_x	CNTs	0.16	31
Co_3O_4/MnO_2	ITO[b]	0.75	14
$Ni(OH)_2$	NFs	0.95	This work

[a]CFP: carbon fiber paper. [b]ITO: indium−tin oxide.

The properties of the present results also are better than those of $Ni(OH)_2$ on other substrates, such as graphene sheets.[32,36] Besides, our results show improved properties compared with NiO_x/carbon nanotubes[37] and Co_3O_4/MnO_2/ITO electrodes.[14] Therefore, the $Ni(OH)_2$ nanoplate arrays may be good candidates for supercapacitors with superior properties.

Figure 5f shows the Ragone plot of the estimated specific energy (E) and specific power (P) at various current densities. The power density and energy density are generally used as important parameters to characterize the electrochemical performance. They can be calculated from the galvanostatic discharge curves using the previous equations (2) and (3). It can be seen that $Ni(OH)_2$ (4 h) has much higher energy densities compared with other $Ni(OH)_2$. As the galvanostatic charge−discharge current increased from 6 to 60 mA/cm^2, the energy densities were 0.906, 0.703, 0.582, and 0.348 Wh/m^2, while the power densities were 14.6, 28.9, 57.6, and 144 W/m^2 at current densities of 6, 12, 24, and 60 mA/cm^2, respectively. The highest energy density (0.906 Wh/m^2) and the highest power density (144 W/m^2) were achieved with slow and fast charge−discharge rates, respectively.[36,38]

Clearly understanding the origin of the high capacitance and stability is important and inspirational for the further construction of practical devices. A schematic illustration of the electrochemical process for the $Ni(OH)_2$ nanoplate arrays grown in 4 h on the NFs was proposed, as shown in Figure 6.

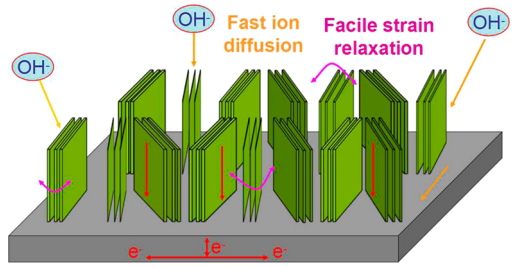

Figure 6. Schematic illustration of the $Ni(OH)_2$ nanoplate arrays (4 h) for fast electron transfer and the diffusion of ions.

This unique interlayer architecture facilitates the soaking of electrolytes into the electrode materials, creates many short-distance paths for ion transportation, and provides more electroactive sites for fast energy storage at large current densities. Meanwhile, each nanoplate, acting as the cells of the structure, contacts with the nickel substrate rather than nickel oxide, avoiding the usage of binders and conducting additives and providing an effective and stable pathway for charge transfer. Finally, the interspaces between the nanoplate arrays contribute to facile strain relaxation and diffusion of ions, alleviating the structure or phase damage caused by the redox reaction during the cycling procedure.

4. CONCLUSIONS

The spike-piece-structured $Ni(OH)_2$ interlayer nanoplate arrays are directly synthesized on a 3D NF by a facile hydrothermal technique. The surface of the NFs, especially the oxide layer, may affect the morphology of $Ni(OH)_2$ nanoplates on the NFs. The composites showed a capacity of 2.83 F/cm^2 at a current density of 6 mA/cm^2. The materials exhibit good cycling performance, with 62.1% and 51.5% of its initial capacity remaining after about 1000 and 3000 charge−discharge cycles at a large current density of 24 mA/cm^2. The good electrochemical properties of the $Ni(OH)_2$ nanoplate arrays (obtained at 4 h) can be attributed to the following aspects. First, the $Ni(OH)_2$ nanoplate arrays present spike-piece structures with large specific surface area, resulting in high specific capacitance. Second, the $Ni(OH)_2$ nanostructure is directly formed on the NFs, providing good electrical contact between the active materials and the substrate. Third, the NFs possess special 3D structure, leading to a large surface area for the growth of abundant $Ni(OH)_2$ and fast diffusion of ions for energy storage at high power. Fourth, the irregular arrays of $Ni(OH)_2$ nanoplates are facile for the fast transfer of ions. Therefore, the above results indicate that this material is an attractive and promising candidate for supercapacitor electrodes.

AUTHOR INFORMATION

Corresponding Authors

*E-mail: liqiuhong2004@hotmail.com.
*E-mail: zhangming@hnu.edu.cn.

Notes

The authors declare no competing financial interest.

ACKNOWLEDGMENTS

This work was partly supported by the National Natural Science Foundation of China (Grants 21003041 and 61376073), the Specialized Research Fund for the Doctoral Program of Higher Education of China (Grant 20120161110016), the Hunan Provincial Natural Science Foundation of China (Grants 10JJ1011 and 11JJ7004), and the Hunan Provincial Major Project of Science and Technology Department (Grant 2012TT1004).

REFERENCES

(1) Yuan, Y. F.; Xia, X. H.; Wu, J. B.; Yang, J. L.; Chen, Y. B.; Guo, S. Y. Nickel foam-supported porous $Ni(OH)_2$/NiOOH composite film as advanced pseudocapacitor material. *Electrochim. Acta* **2011**, *56*, 2627−2632.

(2) Nam, K. W.; Yoon, W. S.; Kim, K. B. X-ray absorption spectroscopy studies of nickel oxide thin film electrodes for supercapacitors. *Electrochim. Acta* **2002**, *47*, 3201−3209.

(3) Hu, C. C.; Cheng, C. Y. Ideally pseudocapacitive behavior of amorphous hydrous cobalt−nickel oxide prepared by anodic deposition. *Electrochem. Solid-State Lett.* **2002**, *5*, A43−A46.

(4) Chen, Y.; Qu, B.; Hu, L.; Xu, Z.; Li, Q.; Wang, T. High-performance supercapacitor and lithium-ion battery based on 3D hierarchical NH_4F-induced nickel cobaltate nanosheet-nanowire cluster arrays as self-supported electrodes. *Nanoscale* **2013**, *5*, 9812−9820.

(5) Nohara, S.; Toshihide, A. A.; Wada, H.; Furukawa, N.; Inoue, H.; Sugoh, N.; Iwasaki, H.; Iwakura, C. Hybrid capacitor with activated carbon electrode, $Ni(OH)_2$ electrode and polymer hydrogel electrolyte. *J. Power Sources* **2006**, *157*, 605−609.

(6) You, Z.; Shen, K.; Wu, Z. C.; Wang, X. F.; Kong, X. H. Electrodeposition of Zn-doped α-nickel hydroxide with flower-like nanostructure for supercapacitors. *Appl. Surf. Sci.* **2012**, *258*, 8117−8123.

(7) Huang, L.; Chen, D.; Ding, Y.; Wang, Z. L.; Zeng, Z.; Liu, M. Hybrid composite $Ni(OH)_2$@$NiCo_2O_4$ grown on carbon fiber paper for high-performance supercapacitors. *ACS Appl. Mater. Interfaces* **2013**, *5*, 11159−11162.

(8) Lu, Z.; Chang, Z.; Zhu, W.; Sun, X. Beta-phased $Ni(OH)_2$ nanowall film with reversible capacitance higher than theoretical Faradic capacitance. *Chem. Commun.* **2011**, *47*, 9651−9653.

(9) Hu, C. C.; Chen, J. C.; Chang, K. H. Cathodic deposition of $Ni(OH)_2$ and $Co(OH)_2$ for asymmetric supercapacitors: Importance of the electrochemical reversibility of redox couples. *J. Power Sources* **2013**, *221*, 128−133.

(10) Xie, J. F.; Sun, X.; Zhang, N.; Xu, K.; Zhou, M.; Xie, Y. Layer-by-layer β-$Ni(OH)_2$/graphene nanohybrids for ultraflexible all-solid-state thin-film supercapacitors with high electrochemical performance. *Nano Energy* **2013**, *2*, 65−74.

(11) Tang, H.; Yin, H.; Wang, J.; Yang, N.; Wang, D.; Tang, Z. Molecular Architecture of Cobalt Porphyrin Multilayers on Reduced Graphene Oxide Sheets for High-Performance Oxygen Reduction Reaction. *Angew. Chem.* **2013**, *125*, 5695−5699.

(12) Liu, J.; Cheng, C.; Zhou, W.; Li, H.; Fan, H. J. Ultrathin nickel hydroxidenitrate nanoflakes branched on nanowire arrays for high-rate pseudocapacitive energy storage. *Chem. Commun.* **2011**, *47*, 3436−3438.

(13) Xing, S.; Wang, Q.; Ma, Z.; Wu, Y.; Gao, Y. Synthesis of mesoporous α-$Ni(OH)_2$ for high-performance supercapacitors. *Mater. Lett.* **2012**, *78*, 99−101.

(14) Liu, J.; Jiang, J.; Cheng, C.; Li, H.; Zhang, J.; Gong, H.; Fan, H. J. Co_3O_4 Nanowire@MnO_2 ultrathin nanosheet core/shell arrays: a new class of high-performance pseudocapacitive materials. *Adv. Mater.* **2011**, *23*, 2076−2081.

(15) Wang, H.; Casalongue, H. S.; Liang, Y.; Dai, H. $Ni(OH)_2$ Nanoplates Grown on Graphene as Advanced Electrochemical Pseudocapacitor Materials. *J. Am. Chem. Soc.* **2010**, *132*, 7472−7477.

(16) Lang, J. W.; Kong, L. B.; Liu, M.; Luo, Y. C.; Kang, L. Asymmetric supercapacitors based on stabilized α-$Ni(OH)_2$ and activated carbon. *J. Solid State Electrochem.* **2010**, *14*, 1533−1539.

(17) Hou, L. R.; Yuan, C. Z.; Li, D. K.; Yang, L.; Shen, L. F.; Zhang, F.; Zhang, X. G. Electrochemically induced transformation of NiS nanoparticles into $Ni(OH)_2$ in KOH aqueous solution toward electrochemical capacitors. *Electrochim. Acta* **2011**, *56*, 7454−7459.

(18) Li, Y.; Yao, J.; Zhu, Y.; Zou, Z.; Wang, H. Synthesis and electrochemical performance of mixed phase α/β nickel hydroxide. *J. Power Sources* **2012**, *203*, 177−183.

(19) Chen, X.; Chen, X.; Zhang, F.; Yang, Z.; Huang, S. One-pot hydrothermal synthesis of reduced graphene oxide/carbon nanotube/α-$Ni(OH)_2$ composites for high performance electrochemical supercapacitor. *J. Power Sources* **2013**, *243*, 555−561.

(20) Lv, S.; Suo, H.; Wang, J.; Wang, Y.; Zhao, C.; Xing, S. Facile synthesis of nanostructured $Ni(OH)_2$ on nickel foam and its electrochemical property. *Colloids Surf. A* **2012**, *396*, 292−298.

(21) Zhang, F.; Zhu, D.; Chen, X. a.; Xu, X.; Yang, Z.; Zou, C.; Yang, K.; Huang, S. A nickel hydroxide-coated 3D porous graphene hollow sphere framework as a high performance electrode material for supercapacitors. *Phys. Chem. Chem. Phys.* **2014**, *16*, 4186−4192.

(22) Zhang, J. T.; Liu, S.; Pan, G. L.; Li, G. R.; Gao, X. P. A 3D hierarchical porous α-$Ni(OH)_2$/graphite nanosheet composite as an electrode material for supercapacitors. *J. Mater. Chem. A* **2014**, *2*, 1524−1529.

(23) Yang, G. W.; Xu, C. L.; Li, H. L. Electrodeposited nickel hydroxide on nickel foam with ultrahigh capacitance. *Chem. Commun.* **2008**, *44*, 6537−6539.

(24) Patil, U. M.; Gurav, K. V.; Fulari, V. J.; Lokhande, C. D.; Joo, O. S. Characterization of honeycomb-like "β-$Ni(OH)_2$" thin films synthesized by chemical bath deposition method and their supercapacitor application. *J. Power Sources* **2009**, *188*, 338−342.

(25) Dubal, D. P.; Fulari, V. J.; Lokhande, C. D. Effect of morphology on supercapacitive properties of chemically grown β-$Ni(OH)_2$ thin films. *Microporous Mesoporous Mater.* **2012**, *151*, 511−516.

(26) Yan, X. Y.; Tong, X. L.; Wang, J.; Gong, C. W.; Zhang, M. G.; Liang, L. P. Rational synthesis of hierarchically porous NiO hollow spheres and their supercapacitor application. *Mater. Lett.* **2013**, *95*, 1−4.

(27) Fan, J. Z.; Mi, H. Y.; Xu, Y. L.; Gao, B. In situ fabrication of $Ni(OH)_2$ nanofibers on polypyrrole-based carbon nanotubes for high-capacitance supercapacitors. *Mater. Res. Bull.* **2013**, *48*, 1342−1345.

(28) Jiang, H.; Zhao, T.; Li, C.; Ma, J. Hierarchical self-assembly of ultrathin nickel hydroxide nanoflakes for high-performance supercapacitors. *J. Mater. Chem.* **2011**, *21*, 3818−3823.

(29) Xiao, T.; Hu, X.; Heng, B.; Chen, X.; Huang, W.; Tao, W.; Wang, H.; Tang, Y.; Tan, X.; Huang, X. $Ni(OH)_2$ nanosheets grown on graphene-coated nickel foam for high-performance pseudocapacitors. *J. Alloys Compd.* **2013**, *549*, 147−151.

(30) Dong, S.; Chen, X.; Zhang, K.; Gu, L.; Zhang, L.; Zhou, X.; Li, L.; Liu, Z.; Han, P.; Xu, H.; Yao, J.; Zhang, C.; Zhang, X.; Shang, C.; Cui, G.; Chen, L. Molybdenum nitride based hybrid cathode for rechargeable lithium-O_2 batteries. *Chem. Commun.* **2011**, *47* (40), 11291−11293.

(31) Nam, K.-W.; Kim, K.-H.; Lee, E.-S.; Yoon, W.-S.; Yang, X.-Q.; Kim, K.-B. Pseudocapacitive properties of electrochemically prepared nickel oxides on 3-dimensional carbon nanotube film substrates. *J. Power Sources* **2008**, *182*, 642−652.

(32) Tang, Z.; Tang, C.-h.; Gong, H. A High Energy Density Asymmetric Supercapacitor from Nano-architectured $Ni(OH)_2$/Carbon Nanotube Electrodes. *Adv. Funct. Mater.* **2012**, *22*, 1272−1278.

(33) Yan, J.; Fan, Z.; Sun, W.; Ning, G.; Wei, T.; Zhang, Q.; Zhang, R.; Zhi, L.; Wei, F. Advanced Asymmetric Supercapacitors Based on $Ni(OH)_2$/Graphene and Porous Graphene Electrodes with High Energy Density. *Adv. Funct. Mater.* **2012**, *22*, 2632−2641.
(34) Shahid, M.; Liu, J.; Shakir, I.; Warsi, M. F.; Nadeem, M.; Kwon, Y.-U. Facile approach to synthesize $Ni(OH)_2$ nanoflakes on MWCNTs for high performance electrochemical supercapacitors. *Electrochim. Acta* **2012**, *85*, 243−247.
(35) Zhang, H.; Chen, Y.; Wang, W.; Zhang, G.; Zhuo, M.; Zhang, H.; Yang, T.; Li, Q.; Wang, T. Hierarchical Mo-decorated Co_3O_4 nanowire arrays on Ni foam substrates for advanced electrochemical capacitors. *J. Mater. Chem. A* **2013**, *1*, 8593−8600.
(36) Tang, C. H.; Yin, X.; Gong, H. Superior performance asymmetric supercapacitors based on a directly grown commercial mass 3D Co_3O_4@$Ni(OH)_2$ core−shell electrode. *ACS Appl. Mater. Interfaces* **2013**, *5*, 10574−10582.
(37) Lin, P.; She, Q.; Hong, B.; Liu, X.; Shi, Y.; Shi, Z.; Zheng, M.; Dong, Q. The Nickel Oxide/CNT Composites with High Capacitance for Supercapacitor. *J. Electrochem. Soc.* **2010**, *157*, A818−A823.
(38) Qu, B.; Chen, Y.; Zhang, M.; Hu, L.; Lei, D.; Lu, B.; Li, Q.; Wang, Y.; Chen, L.; Wang, T. β-Cobalt sulfide nanoparticles decorated graphene composite electrodes for high capacity and power supercapacitors. *Nanoscale* **2012**, *4*, 7810−7816.